IP2016 / 4th International Workshop on Induced Polarization

Airborne IP for Kimberlite Exploration

Douglas W. Oldenburg
University of British Columbia
6339 Stores Rd., Vancouver, Canada
doug@eos.ubc.ca

Seogi Kang
University of British Columbia
6339 Stores Rd., Vancouver, Canada
skang@eos.ubc.ca

SUMMARY

Negative transients in coincident loop airborne time domain electro-magnetic (ATEM) data have often been observed when exploring for kimberlite deposits. It is usually supposed that the negative transients arise from chargeable material such as surficial clays or ice in permafrost. As such, this EM signal is generally regarded as a "problem" in mineral exploration because it distorts the EM signals from the conductive kimberlites, and if not corrected for, results in an incorrect conductivity. However, chargeability could be reflective of the kimberlite, hence the induced polarization (IP) effects can be valuable "signal". The ATEM surveys at the Tli Kwi Cho (TKC) kimberlite complex have been a testbed for illustrating the existence of negative transients and we focus on that region. The two pipes that constitute TKC have been extensively drilled and the resultant geologic models can be used to validate our inversion results. In addition, the complex impedance of TKC core samples have been measured in the laboratory and the results showed that the kimberlites can be chargeable and that different kimberlite units have different IP characteristics. In this paper, we first address the important issue about depth of resolution of buried chargeable bodies relevant to kimberlite exploration. After showing its potential we remove the EM effects from the IP data and invert them to recover 3D distributions of pseudo-chargeability at multiple time channels. The recovered pseudo-chargeability at different times provides meaningful information about the diamondiferous portion of the pipe and distinguishes it from other kimberlitic rocks.

Key words: airborne EM, Induced polarization, Kimberlite, and 3D inversion

INTRODUCTION

Figure 1(a) shows a typical geologic model of a kimberlite composed of three different parts: crater, diatreme, and hypabyssal facies. Physical properties of those three facies are shown in Figure 1(b). Kimberlite exploration has focused on looking for high magnetic susceptibility, low density and high conductivity (Power and Hildes, 2007). The high conductivity is often associated with lake bottom sediments as well as the pyroclastic units at depth. The conductivity of the kimberlites is usually found using airborne EM (AEM) surveys, and in particular airborne time domain EM (ATEM) systems. Often however, negative transients observed (Jansen and Witherly, 2004) indicating there is chargeable material (Weidelt, 1982). Ice and near surface clays are known to be chargeable (Smith and Klein, 1996), and these materials distort the AEM signals and impede ability to extract good information about the conductivity. As such, the existence of chargeable materials is usually considered to be a "problem" and it is referred to as IP contamination. The possibility exists however, that the chargeability is reflective of the kimberlite and it is therefore "signal" that we want to interpret.

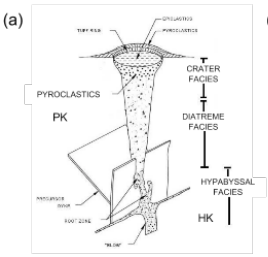

(b)

Rock Type	Suscept-ibility	Density	Conduct-ivity
Hypabyssal & Diatreme facies	High	High	High
Crater facies	Moderate	Low	High
Granitic host rock	Low	Moderate	Low

Figure 1. (a) General structure of kimberlite pipe. (b) Physical properties of geological units in the kimberlite pipe.

The Tli Kwi Cho (TKC) kimberlite complex is located approximately 360 km northeast of Yellowknife, NWT, Canada within the Archean Slave craton. The complex is part of the larger Lac de Gras kimberlite field. The TKC kimberlites are composed of two main pipes called DO-18 and DO-27, and they are respectively located at northern and southern part of the region as shown in Figure 2(a). There are four rock units of importance: XVK (Xenolithic kimberlite), VK (volcaniclastic kimberlite), HK (hypabyssal kimberlite) and PK (pyroclastic kimberlite). DO-18 pipe is mostly XVK and DO-27 is a combination of PK and HK. The PK unit is the sought diamondiferous portion of the pipe. An east-west geological section at DO-27, generated from drilling results (Harder et al., 2006) is shown in Figure 2(b). Petrophysical data including density, susceptibility, Koenigsberger, complex conductivity have been measured from core samples at both pipes. Figure 3 shows the measured complex impedance from TKC core samples corresponding to PK (green), HK (red), and XVK (purple) units.

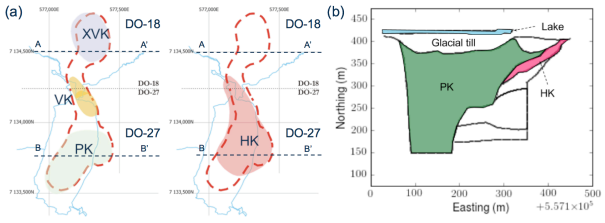

Figure 2. Geological background of Tli Kwi Cho (TKC) Kimberlites. (a) Plan maps of TKC with kimberlite units: PK, HK, VK, and XVK. (b) East-west geological section of DO-27 pipe. The map showing PK is at a shallower depth than the map showing HK.

The impedance plots indicate that the kimberlites are chargeable, and analysis shows that the estimated time constants are different; PK has a much slower decay than HK and XVK. This raises two important questions: a) Can we invert ATEM data for chargeability? and b) Can this provide some meaningful information about the kimberlite?

A major challenge for extracting IP information from airborne data arises from the $1/r^3$ decay of signal away from the source and the fact that the top few tens meters often include permafrost and clay (Macnae, 2015). AIP is thus often thought

of as a 'clay mapper'. Investigation of the depth resolution on AIP is therefore crucial. We will use the geometry of TKC pipes to address this question and then carry through an analysis to extract geologic information from the AIP data. To investigate depth resolution for AIP data we generate synthetic AIP data sets with a chargeable target at different depths and apply a 3D IP inversion to them. To proceed, we briefly outline essential definitions and procedures. Detailed information can be found in Kang and Oldenburg (2016).

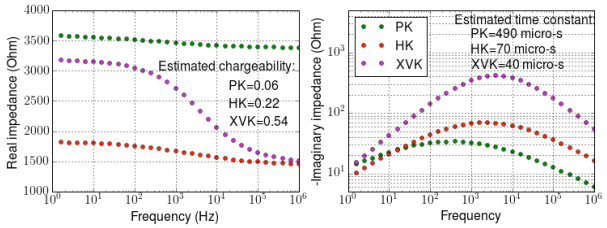

Figure 3. Complex impedance measured from core samples from PK (green), HK (red), and XVK (purple) units. Left and right panel shows real and imaginary parts of the impedance.

COMPLEX CONDUCTIVITY

Complex conductivity in the frequency domain can be expressed as

$$\sigma(\omega) = \sigma_\infty + \triangle\sigma(\omega) \tag{1}$$

where σ_∞ is conductivity at infinite frequency, and ω is angular frequency (rad/s). Different descriptive models exist but, following Smith et al. (1988), we use the Cole-Cole model from Pelton et al. (1978):

$$\triangle\sigma(\omega) = -\sigma_\infty \frac{\eta}{1+(1-\eta)(\imath\omega\tau)^c}, \tag{2}$$

where η is intrinsic chargeability, τ is time constant, and c is frequency dependency.

LINEAR FORM OF IP RESPONSE

An ATEM observation, d^{obs}, includes both EM and IP effects and can be expressed as

$$d^{obs} = d^F + d^{IP}, \tag{3}$$

where the fundamental response is $d^F \equiv F[\sigma_\infty]$, which does not include any IP effects, and d^{IP} is the IP response. Here $F[\cdot]$ indicates Maxwell's operator which takes conductivity and computes a TEM response. The IP datum can be expressed as

$$d^{IP} = d^{obs} - d^F, \tag{4}$$

This procedure can be considered as EM-decoupling because we are removing EM induction effects from the observations. The IP responses can be written in a linear form:

$$d^{IP}(t) = G\tilde{\eta}(t), \tag{5}$$

where G is the sensitivity function and $\tilde{\eta}(t)$ is the pseudo-chargeability. Note that this pseudo-chargeability is time-dependent, but the intrinsic chargeability is not. This linear form will be the forward function that we use to invert IP data.

DEPTH INFORMATION IN AIP

The depth resolution of AIP data is limited because of the geometric decay of the IP signal from a chargeable target. It is often expected that the resolution is only a few tens of meters for a compact target at the surface and about 90 m for chargeable layers (Macnae, 2015). We systematically treat this issue in the context of kimberlite exploration. We consider a circular-shaped chargeable target, which is moderately conductive and embedded in a resistive background. This could correspond to a PK unit or a crater facies (Figure 1a).

Depth resolution of the AIP data includes two important items: detection and delineation. For the first item, using an ATEM survey geometry shown in Figure 1(a), we perform forward modelling and compute db_z/dt (Figure 1b) using the EMTDIP code (Marchant et al., 2014). The half-space earth (10^{-4} S/m) includes a conductive and chargeable cylinder and Cole-Cole parameters of the chargeable unit are $\sigma_\infty=10^{-1}$ S/m, η=0.1, c=0.5 and $\tau=10^3$ micro-s. With fixed thickness (75 m) and radius (100 m) of the cylinder, we alter the depth from the surface as 0, 75, and 150 m. Although the amplitude of the observation decreases with increasing depth, the time at which the negative value appears is almost constant (~700 micro-s) for all three depths. Assuming a noise level of 10^{-3} pV/A-m^2, the detectability level is about 150 m. The cylinders at depths of 75 or 100 meters have numerous time channels of negative values that are well about this threshold. The main difference of the responses at the three depths is just an amplitude factor so it is not likely that depth information can be obtained from a single sounding. In practice, however, we obtain ATEM data from a number of sounding locations.

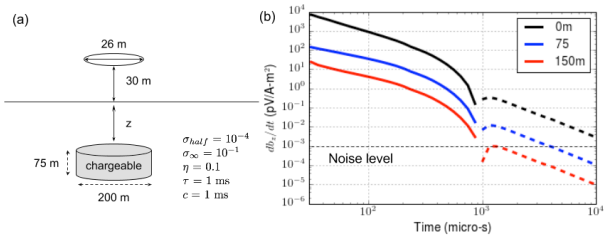

Figure 4. (a) Geometry of an ATEM system, and a chargeable cylinder embedded in the half-space earth. (b) Observed vertical magnetic fields (db_z/dt) with varying depths for the chargeable unit. Solid and dotted lines respectively indicate positive and negative data.

We perform two forward modellings: $F[\sigma]$ (observation) and $F[\sigma_\infty]$ (fundamental) at 210 sounding locations. Then, using Eq. (4), we evaluate the IP data at 1300 micro-s as shown in Figure 5. As the depth increases, the IP responses get broader and smoother due to the geometric effects. Although not shown here, the spatial variation of the IP data hardly changes in time, hence, this is similar to potential field data. Similar to the inversion of magnetic data we apply a depth weighting to compensate for the ($1/r^3$) decay. In the following we carry out 3D IP inversions with, and without, the depth weighting applied to IP data sets where the models had different depths ($z = 0$, 75, and 150 m). Forming the sensitivity function requires a 3D conductivity model, and we used the true conductivity model for each case. Figure 6 shows the recovered pseudo-chargeability models. Based upon these results, resolving depth information looks possible and the depth weighting seems to be advantageous, but not crucial.

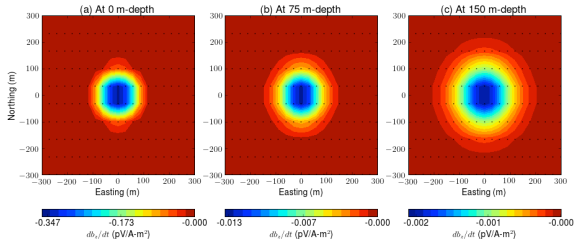

Figure 5. True IP responses computed by subtraction using Eq. (4). Depth of the chargeable cylinder varies: a) 0m, b) 75 m, and c) 150-m depth. Dots indicate horizontal locations of soundings.

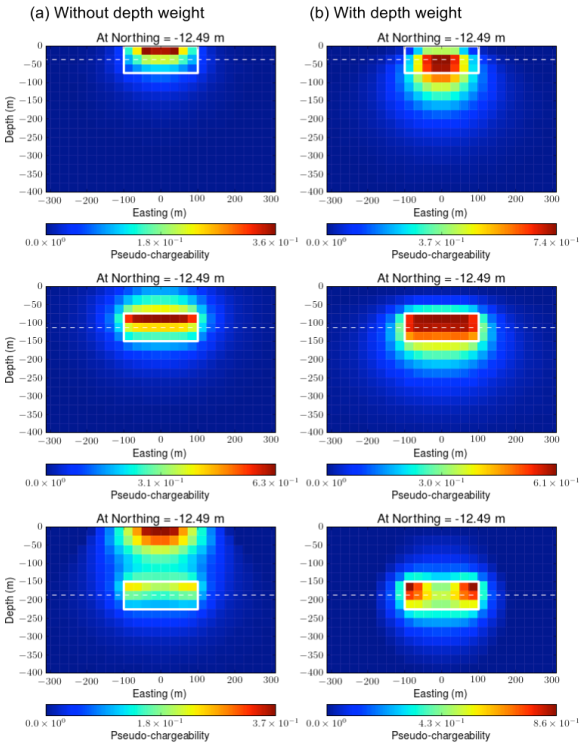

Figure 6. Sections of recovered pseudo-chargeability at different depths. (a) Without depth weighting and (b) with depth weighting. Top, middle, and bottom panel correspondingly indicate a chargeable target at 0, 75, and 150 m-depth.

FIELD EXAMPLE: TKC

TKC ATEM data

Airborne EM surveys flown over TKC include DIGHEM, AeroTEM, and VTEM systems We focus on the VTEM data set because it illustrates the challenges we can encounter when handling AIP data. As shown in Figure 7(a), even at the earliest time (90 micro-s), VTEM data have negative values (dotted contours) over DO-18 and between DO-18 and DO-27. DO-27 shows a positive anomaly (solid contour) at this time, but data become negative at 680 micro-s as shown in Figure 7b. Easting profile lines over DO-18 and DO-27, respectively shown in Figure 7(c) and (d), show the transition.

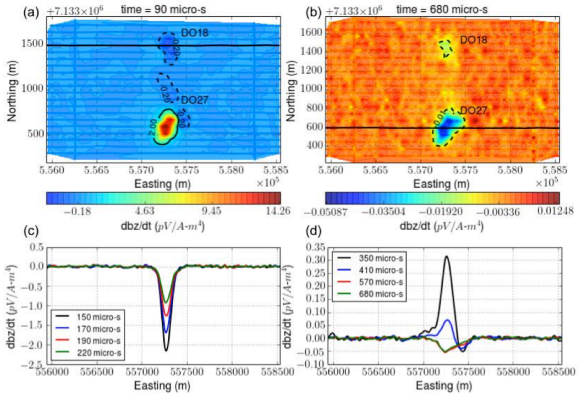

Figure 7. TKC VTEM data. Maps of VTEM responses at (a) 90 micro-s and (b) 680 micro-s. Easting profile line data near (c) DO-18 and (d) DO-27.

3D ATEM and IP inversions

Our approach to invert AIP data is based upon Kang and Oldenburg (2016). The first step is to invert ATEM data to recover the conductivity. To exclude IP effects in the observations, we only use the first 6 time channels of the VTEM data (90-190 micro-s) near DO-27. This cannot be done for VTEM data near DO-18 since even the earliest channel is negative. Fortunately, DIGHEM data covers the entire TKC area and we assume it is not significantly affected by IP, so we cooperatively invert VTEM and DIGHEM data. The recovered 3D conductivity model is shown in Figure 8. At B-B' section, we overlay the boundaries of different kimberlite units obtained from drilling results (Figure 2b). The two conductive pipes are imaged at depth. The pipe for DO-27 extends deeper depth than one for DO-18. The location of recovered conductive pipe at DO-27 matches well with the PK unit.

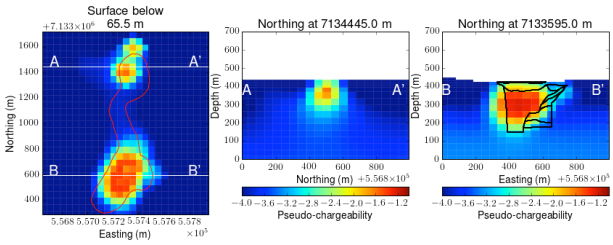

Figure 8. Recovered 3D conductivity model. Left panel shows plan view at 65.5 mbsf. Middle and right panels show section views at Northing 713445m and 7133595m.

Based upon the recovered conductivity, σ_{est}, we proceed with EM-decoupling:

$$d^{IP}_{raw} = d^{obs} - F[\sigma_{est}], \qquad (6)$$

where d^{IP}_{raw} is raw IP data, $F[\sigma_{est}]$ is estimated fundamental data. Figure 9 shows the observed, estimated fundamental response, and raw IP data at 130 and 410 micro-s where both EM and IP effects are substantial. Our EM-decoupling effectively removes EM induction effects due to the conductive pipe at DO-27 at both of the times evaluated here.

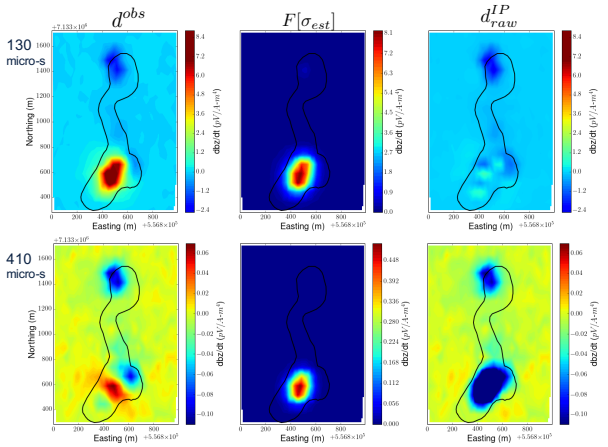

Figure 9. Plan maps of observed (left panel), estimated fundamental (middle panel) and raw IP (right panel) data at 130 (top panel) and 410 (bottom panel) micro-s.

We separately invert each time channel of raw IP data and recover 3D pseudo-chargeability at multiple times. Figure 10. shows recovered pseudo-chargeability at 130 and 410 micro-s. Four chargeable anomalies, A1-A4, are imaged. A1-A3 are imaged at 130 micro-s, whereas A4 is not imaged at that time but is apparent at 410 micro-s. This reflects the different time decays associated with the AIP signals, and it is consistent

with the complex impedance measurements shown in Figure 3 if the A4 anomaly is a PK unit and the other anomalies, A1-A3 are associated with the other kimberlitic rocks. Through a comparison of Figure 10 and Figure 2(a), which was obtained from drilling, it appears that A1, A2, A3, and A4 might respectively be connected to XVK, VK, HK, and PK units. Recalling that PK is the most diamondiferous unit, the recovered pseudo-chargeability at the two different times shows that the PK unit is distinct from three other units: XVK, VK, and HK in 3D space. In particular, at the B-B' section through DO-27 we have overlaid the pseudo-chargeabilty with the geological boundaries. (see right panel of Figure 10.) Comparisons of the boundaries and pseudo-chargeability at 130 and 410 micro-s suggests we are delineating between the PK from HK units.

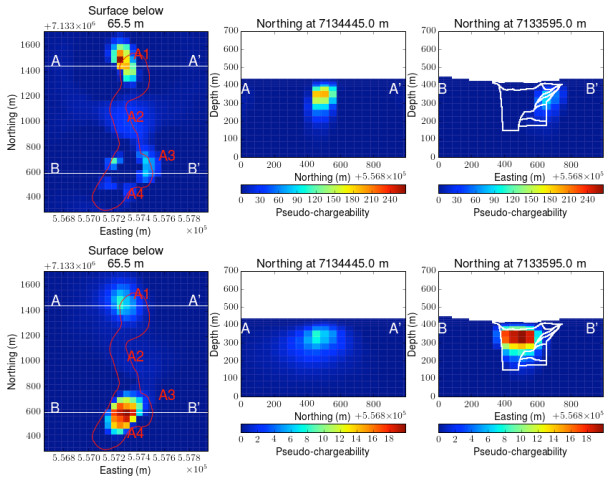

Figure 10. Recovered 3D pseudo-chargeability model at 130 (top row) and 410 (bottom row) micro-s. Left panel shows plan view at 65.5 mbsf. Middle and right panels show section views at Northing 713445m and 7133595m.

CONCLUSIONS

In this paper, we investigated the feasibility of the AIP technique for kimberlite exploration and used the TKC kimberlite region as an example. The area has been extensively drilled and four types of kimberlitic rocks have been found. Lab measurements on core samples showed TKC kimberlites are chargeable and that they have different IP parameters. This promoted two important questions: a) Can we invert ATEM data for chargeability at depth? and b) Can the results provide meaningful information about the kimberlite? Through the use of a synthetic model that emulates a TKC pipe, we analyzed the depth resolution issue and found that targets buried 75-100 meters might still be detectable and that inversion that included a depth weighting was beneficial, but might not be crucial.

We applied a 3D ATEM-IP inversion workflow to TKC VTEM data. To recover conductivity, we inverted early time channels of VTEM data (presumed to have insignificant IP-contamination) cooperatively with DIGHEM data. The details for that result will be published in a separate paper. The recovered conductivity includes two moderately conductive pipes near DO-18 and DO-27. The conductivity was used to estimate the fundamental EM response which was subtracted from the data to generate raw IP data at multiple time channels. 3D IP inversions were carried out and the pseudo-chargeabilities at multiple times were obtained. Four chargeable anomalies are imaged at depths (~70 m): A1-A4 possibly correspond to four different kimberlites: XVK, VK, HK and PK. These correspondences can be inferred by comparing the recovered chargeability with geologic logging in boreholes. The recovered pseudo-chargeability at different times suggests a distinction between the PK unit and the other three kimberlite units. Moreover, the outline of the inferred PK unit matches well with the boundaries of the PK unit obtained from drilling, but some of this is likely attributed to the conductivity model and the fact that IP sensitivities are enhanced in regions of higher conductivity. From a geologic perspective, the two main results might be the differentiation of rocks associated with the two pipes. The XVK unit comprising DO-18 is substantially different from the dominant PK unit at DO-27. On a smaller scale, we appear to be able to differentiate between the PK and HK units at DO-27. This is potentially important since PK is strongly diamondiferous and HK has minimal diamond showings. This discrimination might be further enhanced through the use of ground IP using either galvanic or inductive sources. Overall, our study of AIP shows the potential benefits in kimberlite exploration, and hence motivates further research and application in other geoscience problems.

ACKNOWLEDGEMENTS

We thank Ken Witherly and Joel Jansen who provided the motivation and ATEM data to carry out this research, and Brook Clements and Jennifer Pell of Peregrine for providing data and cores for lab measurements. We thank Dom Fournier and Mike McMillan for their contribution to the development of the conductivity model, and Randy Enkin of Gelogical Survey of Cananda, Thibaut Astic, Devin Cowan and others at UBC-GIF for participating in lab measurements and in extensive discussions about TKC.

REFERENCES

Jansen, J., and K. Witherly, 2004, The Tli Kwi Cho kimberlite complex, Northwest Territories, Canada: A geophysical case study: SEG Technical Program Expanded Abstracts, 1147–1150.

Kang, S., and D. W. Oldenburg, 2016, On recovering distributed IP information from inductive source time domain electromagnetic data (in revision): Geophysical Journal International.

Macnae, J., 2015, Quantifying Airborne Induced Polarization effects in helicopter time domain electromagnetics: Journal of Applied Geophysics.

Marchant, D., E. Haber, and D. Oldenburg, 2014, Three-dimensional modeling of IP effects in time-domain electromagnetic data: Geophysics, 79, E303–E314.

Power, M., and D. Hildes, 2007, Geophysical strategies for kimberlite exploration in northern Canada: Proceedings of Exploration '07: Fifth Decennial International Conference on Mineral Exploration, 1025–1031.

Smith, R. S., and J. Klein, 1996, A special circumstance of airborne induced polarization measurements: Geophysics, 61, 66–73.

Smith, R. S., P. Walker, B. Polzer, and G. F. West, 1988, The time-domain electromagnetic response of polarizable bod- ies: an approximate convolution algorithm: Geophysical Prospecting, 36, 772–785.

Weidelt, P., 1982, Response characteristics of coincident loop transient electromagnetic systems: 47, 1325–1330.